*J. Synchrotron Rad.* (1999). **6**, 43–49

# Pressure and temperature dependence of EXAFS Debye–Waller factors in diamond-type and white-tin-type germanium

**Akira Yoshiasa,[a]* Takaya Nagai,[a] Osamu Ohtaka,[a] Osamu Kamishima[b] and Osamu Shimomura[c]**

*[a]Graduate School of Science, Osaka University, Toyanaka 560-0043, Japan, [b]Faculty of Science, Okayama University, Okayama 700-0082, Japan, and [c]JAERI-RIKEN SPring-8 Project Team, Hyogo 678-1298, Japan. E-mail: yoshiasa@ess.sci.osaka-u.ac.jp*

(*Received 24 July 1998; accepted 16 September 1998*)

Extended X-ray absorption fine-structure (EXAFS) spectra near the Ge *K*-edge in diamond- and white-tin-type Ge under high temperature and high pressure were measured using a cubic-anvil-type apparatus (MAX90) with synchrotron radiation from the Photon Factory, Tsukuba, Japan. Pressure values up to 10.6 GPa were estimated on the basis of the isothermal equation of state of the diamond-type Ge within an accuracy of 0.4 GPa. Pressures for the same cell assembly were also determined by X-ray diffraction experiment using the NaCl scale. The diamond-type Ge is of great advantage to the pressure calibrant of EXAFS measurements at elevated temperature because a harmonic approximation can be applied up to 900 K. By the phase transition from diamond- to white-tin-type phases, with an increase in coordination number, Ge—Ge distances increase. A sixfold-coordinated Ge atom in the white-tin-type structure has crystallographically non-equivalent two kinds of nearest-neighbour distances [2.530 (8) Å and 2.697 (8) Å at 12.8 GPa]. The harmonic effective interatomic potential, $V(u) = 1/2\alpha u^2$, was evaluated from the contribution to the thermal vibration, where $u$ is the deviation of the bond distance from the location of the potential minimum. The potential coefficient, $\alpha$, at 0.1 MPa is essentially temperature independent and is 9.06 eV Å$^{-2}$. At 9 GPa the potential coefficient is 9.71 eV Å$^{-2}$. The effective interatomic potential is influenced not only by pressure but also by changes in coordination number. The high-pressure white-tin-type phase has a broader potential and a relatively larger mean square amplitude of vibration than the diamond-type phase.

**Keywords: EXAFS; high pressure; Debye–Waller factor; pressure calibration; diamond-type Ge; white-tin-type Ge; effective interatomic potential.**

## 1. Introduction

Extended X-ray absorption fine-structure (EXAFS) spectroscopy is a useful method for structural investigation around a particular kind of atom in materials such as crystalline, amorphous and liquid phases under high pressure and high temperature (Shimomura & Kawamura, 1987). The distances between an X-ray absorbing atom and its neighbours under pressure can be obtained directly, even if the crystal structure is unknown. The local compressibility of a single bond in complex materials usually differs from the bulk compressibility. The compressibility of a coordination polyhedron of an X-ray absorbing atom can be determined by EXAFS. Some EXAFS studies on crystalline and amorphous Ge under pressure have already been presented in the literature (Kawamura *et al.*, 1981; Shimomura & Kawamura, 1987; Freund *et al.*, 1990). It was demonstrated by Freund *et al.* (1990) that the local compressibility of a single Ge—Ge bond in amorphous Ge is about 30% smaller than the bulk compressibility of the crystalline phase.

The compressibilities of local single bonds and the bulk are the same in such simple crystal structures as NaCl, CsCl, diamond, zinc blende, fluorite, cubic perovskite *etc.* We can use these materials as pressure calibrants for high-pressure EXAFS studies. Freund *et al.* (1989) focused on the method of determining pressure from EXAFS for a material whose isothermal equation of state is well known and whose compressibility is large. Ingalls *et al.* (1980) considered the possibility of applying NaBr and Ge to pressure calibrants for high-pressure EXAFS studies. Although the alkali halides fulfill the criteria for pressure calibrants, the anharmonic contribution to the EXAFS Debye–Waller factor is significant at room temperature (Yoshiasa *et al.*, 1997). It is known that an anharmonic contribution to the Debye–Waller factor appears pronouncedly when the magnitude of the EXAFS Debye–Waller factor is greater than ~0.01 Å$^2$ (Yoshiasa *et al.*,

1997). The accuracy of derived bond distances in alkali halides at room temperature is poorer than that of harmonic materials because the correlation in calculations between the bond distance and the anharmonic term, which has a relatively large error, is large. Copper is an excellent pressure marker in EXAFS experiments with errors of ~0.2–0.5 GPa (Freund *et al.*, 1989), whereas the anharmonic contribution becomes significant in Cu at higher temperatures (Yokoyama *et al.*, 1989). The diamond-type Ge is applicable to the pressure calibration up to 11 GPa though the compressibility of Ge is relatively smaller than that of alkali halides and copper. Ge is of great advantage to the pressure calibrant of EXAFS measurements at elevated temperature because a harmonic approximation can be applied up to 900 K.

EXAFS spectroscopy also provides important information on the thermal vibration. The Debye–Waller factor determined by EXAFS spectroscopy for the first-nearest-neighbour distance is sensitive to short-range correlations of the atomic motion: the mean square relative displacement of the backscattering atoms with respect to the absorbing atom can be determined by EXAFS spectroscopy (Beni & Platzman, 1976; Ishii, 1992). Many studies have explored the possibility that EXAFS provides an effective interatomic potential (Yokoyama *et al.*, 1989; Yoshiasa *et al.*, 1997; Kamishima *et al.*, 1997) with a temperature-independent shape. Recently, EXAFS spectroscopy results have been utilized as a reliability test for the interatomic potentials in molecular dynamics simulations (Dalba *et al.*, 1994; Yashiro *et al.*, 1997).

The vibrational motion of the pair of atoms depends on the lattice type and chemical bonding (Yoshiasa *et al.*, 1997). Vibrational properties and the effective interatomic potential in a material are affected largely by the change in coordination number at a phase-transition point (Yoshiasa *et al.*, 1998). The analysis of pressure- and temperature-dependent EXAFS spectra can yield detailed information on phase transitions accompanying changes in coordination numbers and vibrational properties. It is interesting to know how the effective interatomic potential varies with pressure and coordination environment. The diamond-type Ge transforms into the white-tin-type structure under pressure (Jamieson, 1963). At the phase-transition points the coordination number of Ge changes from four to six.

It is difficult to obtain a wide $k$ range of EXAFS spectra with high resolution using a diamond anvil cell because the Bragg reflections of single-crystal diamond anvils interfere with the EXAFS signals and suddenly reduce the transmitted intensity (Shimomura & Kawamura, 1987). In this study we have measured precise EXAFS spectra under high pressure and high temperature using a cubic-anvil-type apparatus by which we can attain a large sample volume and avoid the Bragg reflections. We have investigated the accuracy of EXAFS analysis under high pressure and demonstrated the pressure effect on the effective interatomic potential. The characteristics of local structure of vibration for diamond- and white-tin-type Ge are discussed.

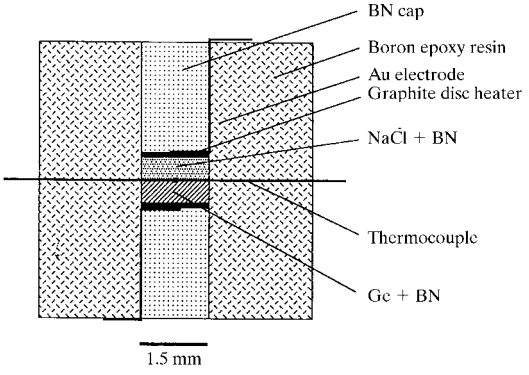


**Figure 1**
Schematic cross-sectional view of the cell assembly.

## 2. Experimental and analysis

Single crystals of diamond-type Ge were synthesized by vapour-phase growth. The crystals were ground into fine powder using an agate mortar. All X-ray absorption measurements near the Ge $K$-edge were made in the transmission mode with synchrotron radiation from the Photon Factory of the National Laboratory for High Energy Physics, Tsukuba, Japan. The ring operating condition was 2.5 GeV and 300 mA. All samples had edge-jumps of 0.7 ($\Delta\mu d$), where $\mu$ is the linear absorption coefficient and $d$ is the thickness. The photon energy, $E$, was calibrated with a Cu foil by assigning 8.9788 keV to the pre-edge peak of the absorption. The intensities of the incident and transmitted X-rays were measured by ionization chambers.

EXAFS experiments for the diamond-type Ge at 0.1 MPa in the temperature range 23–1000 K were performed at beamline 10B. X-rays were monochromated by an Si(311) channel-cut monochromator. The appropriate amounts of sample and boron nitride powder were mixed and pressed into pellets of thickness 0.5 mm and diameter 10.0 mm. The size of the incident X-ray beam was $0.7 \times 7.0$ mm$^2$.

A cubic-type multi-anvil apparatus named MAX90 (Shimomura *et al.*, 1992) was used for the EXAFS study under pressure in the temperature range 300–700 K. Sintered-diamond anvils with a square flat of $3 \times 3$ mm$^2$ were used. A schematic cross-sectional view of the cell assembly is shown in Fig. 1. The pressure-transmitting medium was a 4:1 mixture of amorphous boron and epoxy resin. The appropriate amounts of fine powder sample and boron nitride powder were put into the pressure-transmitting medium. This experiment was performed at beamline 13B2. The synchrotron radiation was monochromated by an Si(111) double-crystal monochromator. The size of the incident X-ray beam was reduced to $0.3 \times 0.3$ mm$^2$. The X-ray intensities were measured for 5 s for

each of 580 points from several tens of electronvolts below each absorption edge to about 1.2 keV above.

The EXAFS interference function, $\chi(k)$, was extracted from the measured absorption spectra using the standard procedure (Maeda, 1987), where $k$ denotes the wave number of photoelectrons, $k = [2m(E - E_0)/\hbar^2]^{1/2}$. $\chi(k)$ was normalized using MacMaster coefficients according to the EXAFS workshop report (Lytle *et al.*, 1989). Fig. 2 shows the Fourier transforms of the EXAFS of Ge at 0.0 GPa (300 K), 11.8 GPa (300 K) and 10.0 GPa (700 K). The largest peak in the radial structure functions $\varphi_{AB}(R)$, obtained by the Fourier transform of $k^3\chi(k)$ for the corresponding edges, was considered to be almost the distance from the absorbing atom to the nearest-neighbour atoms. In quantitative analyses we carried out the Fourier-filtering technique and a non-linear least-squares fitting method by comparing the observed $\chi(k)_{\rm exp}$ and calculated $\chi(k)_{\rm calc}$. Because multiple-scattering effects are absent in the first-nearest-neighbour coordination shell (Stern *et al.*, 1980; Dalba *et al.*, 1994), we used the EXAFS formula in the single-scattering theory with harmonic approximation (Ishii, 1992)

$$\chi(k) = \sum_B (N_B/kR_{AB}^2)|f_B(k,\pi)| \exp[-2R_{AB}/(k/\eta)] \times \exp[-2\sigma(2)k^2] \sin[2kR_{AB} + \psi_{AB}(k)],$$

where $N_B$ is the coordination number of scattering atoms $B$ at distance $R_{AB}$ from the absorbing atom $A$, $|f_B(k,\pi)|$ is the backscattering amplitude of photoelectrons and $\psi_{AB}(k)$ is the phase-shift function. Values of the function $|f_B(k,\pi)|$ and $\psi_{AB}(k)$ were calculated using the *FEFF3* program (Rehr *et al.*, 1991). The Debye–Waller term, $\sigma(2)$, indicates the mean square relative displacement between the absorbing atom and backscattering atoms. The mean free path, $\lambda$, of the photoelectron is assumed to depend on the wave number, $\lambda(k) = k/\eta$, where $\eta$ is a constant.

Because no evident temperature and pressure dependence for $\eta$ and $\Delta E_0$ in each phase was revealed in this experimental resolving power, we assumed that $\eta$ and $\Delta E_0$ have negligible pressure dependence in this pressure range. Here, $\Delta E_0$ is the difference between the theoretical and experimental threshold energies. Changes in $\eta$ and $\Delta E_0$ were taken into account after phase transition. The values of $\eta$ and $\Delta E_0$ for the diamond- and white-tin-type structures are determined so as to give the best fit to the spectrum under pressures of 1 bar and 11.4 GPa, respectively, at 300 K. Single-shell fitting was carried out in the diamond-type structure, where the number of neighbouring atoms was fixed at the crystallographic value as $N_B = 4$. Double-shell fitting was carried out in the white-tin-type structure, where the number of neighbouring atoms was fixed as $N_{B1} = 4$ and $N_{B2} = 2$. The refinement was performed to the structure parameters $R$ and $\sigma(2)$ in each shell by use of the fixed $\eta$ and $\Delta E_0$ values.

On the parameter fitting, according to the EXAFS workshop report (Lytle *et al.*, 1989), the calculated EXAFS function was also filtered by the same method as was used for the observed function in order to eliminate truncation effects through the Fourier transform of the data. The equal deformation of the observed and calculated EXAFS function improves the accuracy of the parameter fitting. The reliability of fit parameters,

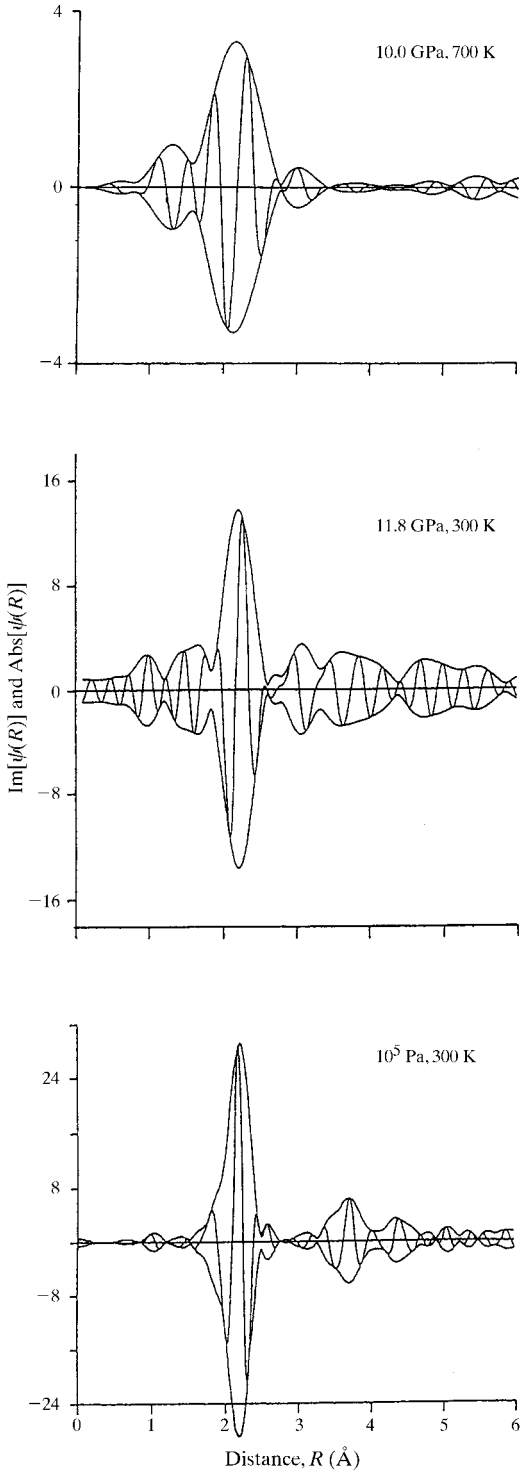


**Figure 2**
Magnitude of the Fourier transform of EXAFS for Ge measured at $10^5$ Pa (1 bar) and 300 K (diamond type), 11.8 GPa and 300 K (white-tin type) and 10.0 GPa and 700 K (white-tin-type structure). The EXAFS phase shift has not been removed.

$$R = \sum_s |k_s^3\chi(k_s)_{\rm exp} - k_s^3\chi(k_s)_{\rm calc}|/|k_s^3\chi(k_s)_{\rm exp}|,$$

between the experimental and calculated EXAFS functions was less than 0.056. The quality of fit between $k^3\chi_{\rm exp}$ and $k^3\chi_{\rm calc}$ is shown in Fig. 3.

## 3. Results and discussion

### 3.1. *Temperature dependence of the Ge—Ge distance in the diamond-type structure*

Fig. 4 shows the temperature dependence of the Ge—Ge nearest-neighbour distance at 0.1 MPa. The temperature dependence of the distance is consistent with the curvature derived from the literature (Singh, 1968; Touloukian *et al.*, 1970). The errors for the distances, which were estimated from statistical fitting errors, were approximately 0.002 Å. It should be considered that the relative comparison of the results provides precision to probe the thermal expansion, though experimental uncertainty at each point is larger than the thermal expansion in the temperature range 100–300 K.

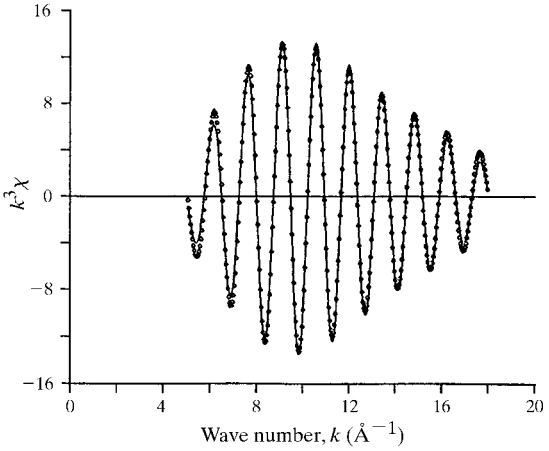


**Figure 3**
Fourier-filtered EXAFS spectra (dotted curve) and least-squares fits (solid curve) for first-nearest Ge—Ge distance at 223 K.

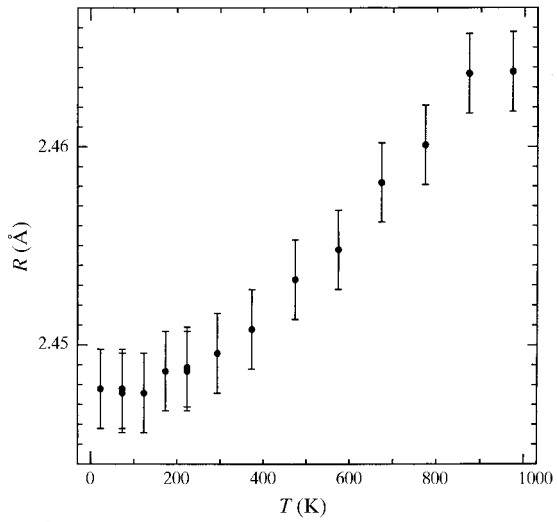


**Figure 4**
Temperature dependence of the Ge—Ge nearest-neighbour distance in Ge under ordinary pressure.

### 3.2. *Pressure calibration*

Pressure values up to 10.6 GPa were estimated on the basis of the two-parameter isothermal equation of state of the diamond-type Ge. We took the values of the bulk modulus at zero pressure, $B_0$ = 73.5 GPa, and its first pressure derivative, $B_0'$ = 4.4 (Freund *et al.*, 1990). The cell volumes were calculated by the nearest-neighbour distances of Ge—Ge in the diamond-type Ge. The nearest-neighbour Ge—Ge distance becomes shortened by about 0.009 Å GPa$^{-1}$. The accuracies in the nearest-neighbour distances under pressure were about 0.003 Å. The relative precision of the bond length should be undoubtedly high, despite some uncertainty in absolute value. Pressures can be determined within an accuracy of 0.4 GPa, if we refer to the atmospheric pressure state as standard.

The pressures for the same cell assembly were determined by X-ray diffraction (XRD) using the NaCl scale (Ohtaka *et al.*, 1998), although the present system could not measure EXAFS and XRD simultaneously. Fig. 5 shows the relations between oil pressure and estimated pressures, which were derived from EXAFS measurements of Ge and XRD measurements of NaCl. The difference between EXAFS and XRD measurements is within 0.4 GPa.

### 3.3. *Phase transition to the white-tin-type structure*

Because X-ray absorption near-edge structure (XANES) spectra of which the energy range is less than 100 eV are quite sensitive to electronic states and three-dimensional atomic configuration around X-ray absorbing atoms, they are easy to use for phase study under high temperature and high pressure. XANES spectra clearly change through the phase transition to the white-tin-type structure accompanying an increase in coordination number. The diamond-type Ge transforms to the white-tin-type structure under a pressure of 11.0 GPa at 300 K. The phase transition is observed under a pressure of 10 GPa at a temperature

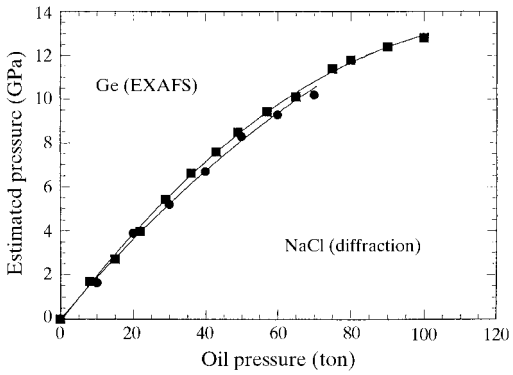


**Figure 5**
Relation between oil pressure and estimated pressure, derived from EXAFS measurements of Ge and XRD measurements of NaCl.

**Table 1**
Pressure dependence of the Ge—Ge distances, $R_{Ge-Ge}$, and Debye–Waller factors, $\sigma(2)$, at 300 K.

| Diamond-type structure [$\eta$ = 0.88 (2) Å$^{-2}$, $\Delta E_0$ = 3.8 (3) eV] | | | White-tin-type structure [$\eta$ = 1.1 (1) Å$^{-2}$, $\Delta E_0$ = 6 (1) eV] | | |
|---|---|---|---|---|---|
| $P$ (GPa) | $R_{Ge-Ge}$ (Å) | $\sigma(2)$ (Å$^2$) | $P$ (GPa) | $R_{Ge-Ge}$ (Å) | $\sigma(2)$ (Å$^2$) |
| 0.0 | 2.447 (3) | 0.00436 (7) | 11.4 | 2.550 (10) | 0.0090 (5) |
| 0.7 | 2.440 (3) | 0.00495 (7) | | 2.713 (12) | 0.0170 (11) |
| 1.6 | 2.429 (4) | 0.00433 (8) | | | |
| 2.6 | 2.419 (3) | 0.00463 (8) | 11.8 | 2.545 (7) | 0.0088 (4) |
| 4.0 | 2.407 (3) | 0.00445 (7) | | 2.701 (9) | 0.0183 (10) |
| 5.6 | 2.394 (3) | 0.00394 (8) | | | |
| 6.8 | 2.384 (3) | 0.00375 (7) | 12.4 | 2.539 (7) | 0.0088 (7) |
| 8.0 | 2.376 (3) | 0.00426 (10) | | 2.707 (8) | 0.0184 (9) |
| 9.0 | 2.369 (4) | 0.00396 (9) | | | |
| 9.9 | 2.362 (3) | 0.00389 (10) | 12.8 | 2.530 (6) | 0.0080 (8) |
| 10.6 | 2.357 (4) | 0.00785 (10) | | 2.697 (8) | 0.0168 (8) |

between 400 and 500 K (Fig. 6). Fig. 7 shows the phase diagram proposed by Vaidya *et al.* (1969) and Shimomura (1996). The phase diagram is consistent with the present results.

The diamond-type Ge is transformed into the white-tin-type structure at about 11 GPa. Therefore, the pressure values over 11 GPa were estimated by extrapolating the relation between the loading oil pressures and the generated pressure up to 10 GPa. The parameters obtained by the least-squares fitting of the data under pressure are listed in Table 1. Across the phase-transition point to the high-pressure phase, with an increase in coordination numbers, Ge—Ge distances increase. A sixfold-coordinated Ge atom in the white-tin-type structure has two kinds of nearest-neighbour distances which are crystallographically non-equivalent with each other. The four Ge—Ge bonds of 2.530 (8) Å are shorter than the other two bonds of 2.697 (8) Å at 12.8 GPa.

### 3.4. *Temperature and pressure dependence of the Debye–Waller factor*

Fig. 8 shows the temperature dependence of the Debye–Waller-type factor, $\sigma(2)$, under a pressure of 0.1 MPa. Harmonic approximation can be applied up to 873 K, which agrees with the result of Crozier & Seary (1981). The values of $\sigma(2)$ from 123 to 873 K follow a straight line. In the low-temperature region, zero-point vibration is predominant. The variable $\sigma(2)$ includes the effects of static and dynamic disorders. The static disorder is the configuration disorder, while the dynamic disorder arises from the thermal vibration of atoms. In addition, there is a correlation in calculation between $\sigma(2)$ and the mean free path, $\lambda$, of the photoelectron. If we assume that a straight line with the same gradient passes through the origin, the

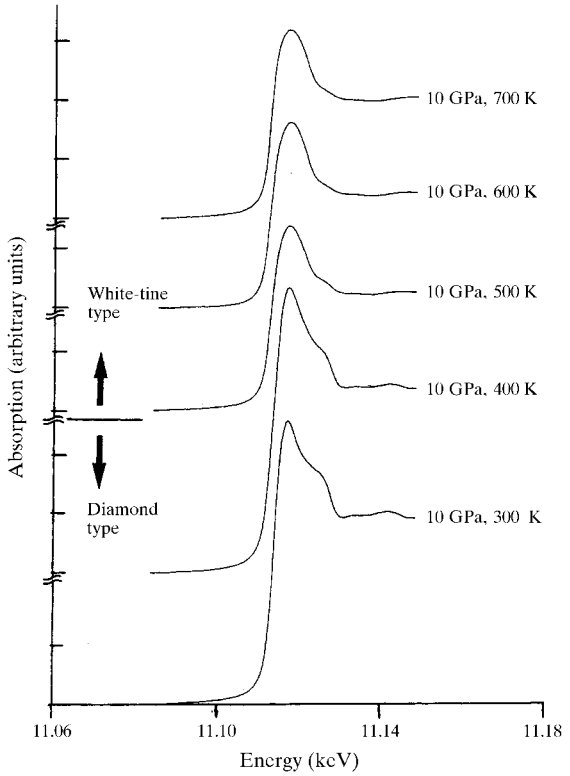


**Figure 6**
Experimental Ge *K*-edge XANES spectra of the diamond- and white-tin-type structures under high pressure and high temperature. The shape of the XANES part' clearly changes above 500 K.

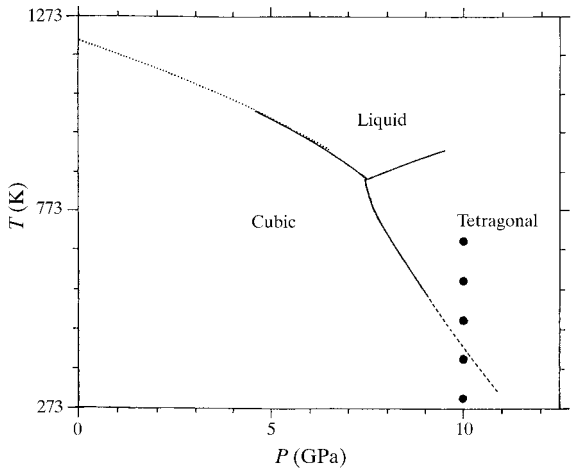


**Figure 7**
Phase diagram of Ge (Shimomura, 1996). Solid circles indicate the measured points depicted in Fig. 6. Full line: Shimomura (1996). Dotted line: Vaidya *et al.* (1969).

deviation of the absolute values is attributed to static disorder and to correlation between $\sigma(2)$ and $\lambda$. The contribution of the thermal vibration (the straight line in Fig. 8), $\sigma_{thermal}$, can be extracted from $\sigma(2)$. The same deviation from the values estimated under the assumption of classical statistical dynamics is observed in other studies (Yokoyama *et al.*, 1989).

We can evaluate the harmonic effective interatomic potential, $V(u) = 1/2\alpha u^2$, from the contribution to the thermal vibration ($\sigma_{thermal}$), where $u$ is the deviation of the bond distance from the location of the potential minimum. The variable $\sigma_{thermal}$ is related to the potential coefficient, $\alpha = k_B T/\sigma_{thermal}$, where $k_B$ is the Boltzmann constant. The potential coefficient, $\alpha$, derived from the gradient for the experimental $\sigma(2)$ in Fig. 8, is essentially temperature independent and is 9.06 eV Å$^{-2}$.

We can also check the validity of the value $\alpha$. We try to estimate the phonon dispersion relations using the potential coefficient $\alpha$ by calculating the dynamical matrix. Details of the calculation were given by Kamishima *et al.* (1997). The phonon dispersion relations along [100], [110] and [111] are shown in Fig. 9 along with the experimental data obtained by neutron inelastic scattering (Nilsson & Nelin, 1971). Since our model consists only of central-force interaction with nearest-neighbour atoms, the acoustic branches degenerate. These calculated phonon energies for Ge are consistent with the values determined by inelastic neutron scattering. The calculated optical phonon energies, which are the most effective in $\sigma_{thermal}$, are consistent with the experimental values. Thus, the potential coefficient $\alpha$ = 9.06 eV Å$^{-2}$ is reasonable.

The decrease in $\sigma(2)$ between 0.1 MPa and 9 GPa was found to be 0.0004 Å$^2$ (Table 1 and Fig. 10). At 9 GPa, the potential coefficient $\alpha$ is 9.71 eV Å$^{-2}$ and the calculated optical phonon energy at the zone boundary is 38.6 meV. The pressure dependence of $\sigma(2)$ corresponds to a raising of the phonon frequencies. The potential is influenced by pressure and becomes steeper with increasing pressure.

The value of the Debye–Waller factor, $\sigma(2)$, at the same pressure with different runs varies within 0.0005 Å$^2$. As shown in Fig. 10, the scatter of absolute values under pressures at 300 K is also 0.0005 Å$^2$, which is significantly larger than that observed in the temperature-dependent experiment. Non-hydrostatic pressure in a multi-anvil cell may be one of the reasons for this. Further experiments at

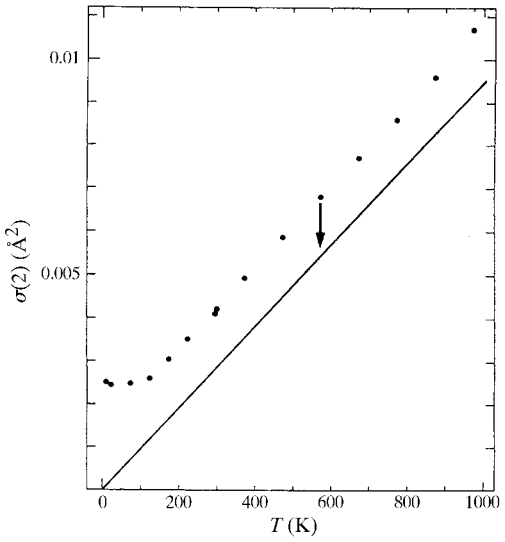


**Figure 8**
Temperature dependence of the Debye–Waller factor, $\sigma(2)$, in Ge. The straight line indicates the contribution of the thermal vibration, $\sigma_{thermal}$. The deviation (arrows) is attributed to static disorder and to correlation between $\sigma(2)$ and $\lambda$.

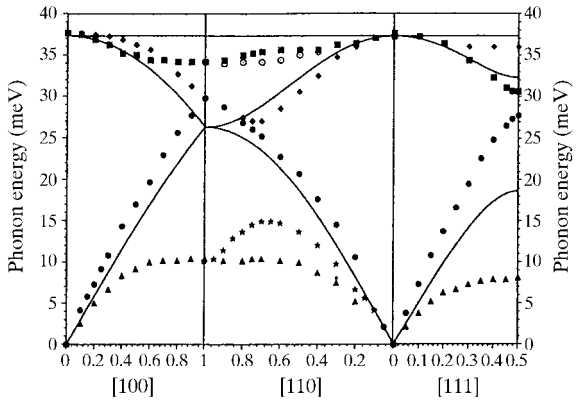


**Figure 9**
Comparison of the calculated phonon dispersions of Ge with experimental data (Nilsson & Nelin, 1971). The solid lines are derived from the EXAFS measurements. $\alpha$ = 9.06 eV Å$^{-2}$. The different symbols indicate individual branches.

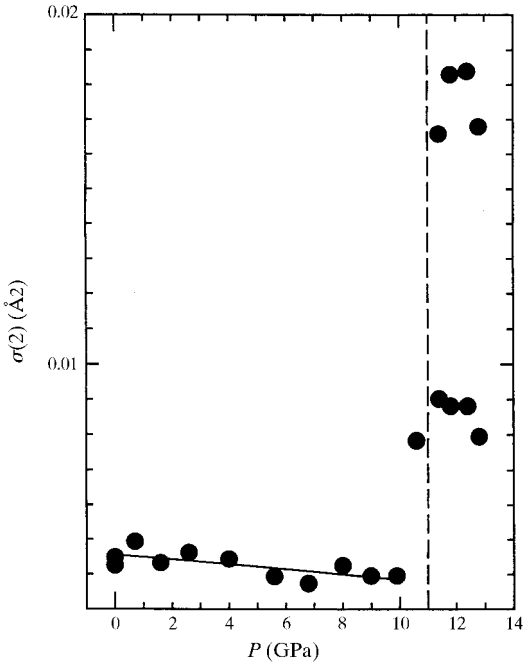


**Figure 10**
Pressure dependence of $\sigma(2)$ in diamond and white-tin-type Ge at 300 K. The diamond-type Ge transforms to the white-tin-type structure under a pressure of 11.0 GPa.

elevated temperature to release strain are necessary and now in progress.

The magnitudes of $\sigma(2)$ in the sixfold-coordinated white-tin-type structure are larger than those in the fourfold-coordinated diamond-type structure (Fig. 10). This means that the effective interatomic potential for the sixfold-coordinated Ge is broader than that for the fourfold-coordinated Ge. The effective interatomic potential is influenced not only by pressure but also by changes in coordination numbers (Yoshiasa *et al.*, 1998). The high-pressure white-tin-type phase has broader potential and a relatively larger mean square amplitude of vibration than the diamond-type phase. The structure changes in the high-pressure phase with an increase in coordination numbers and prolonged bonding distances make the bonds to the first nearest neighbours weaker and affect the vibrational spectra. The number of low-frequency vibrations increases, giving rise to an increase in vibrational entropy. The increase in entropy is responsible for the negative $dP/dT$ slope of the phase boundary between the diamond- and white-tin-type Ge (Fig. 7).

This work was performed under the approval of the Photon Factory Advisory Committee (Proposal No. 95-G333).

## References


Beni, G. & Platzman, P. M. (1976). *Phys. Rev. B*, **14**, 1514–1518.

Crozier, E. D. & Seary, A. J. (1981). *Can. J. Phys.* **59**, 876–882.

Dalba, G., Fornasini, P., Gotter, R., Cozzini, S., Ronchetti, M. & Rocca, F. (1994). *Solid State Ion.* **69**, 13–19.

Freund, J., Ingalls, R. & Crozier, E. D. (1989). *Phys. Rev. B*, **17**, 12537–12547.

Freund, J., Ingalls, R. & Crozier, E. D. (1990). *J. Phys. Chem.* **94**, 1087–1090.

Ingalls, R., Crozier, E. D., Whitmore, J. E., Seary, A. J. & Tranquada, J. M. (1980). *J. Appl. Phys.* **51**, 3158–3163.

Ishii, T. (1992). *J. Phys. Condens. Matter*, **4**, 8029–8034.

Jamieson, J. C. (1963). *Science*, **139**, 762–764.

Kamishima, O., Ishii, T., Maeda, H. & Kashino, S. (1997). *Jpn. J. Appl. Phys.* **36**, 247–253.

Kamishima, O., Ishii, T., Yoshiasa, A., Maeda, H. & Kashino, S. (1997). *J. Phys. IV*, **7**(C2), 255–256.

Kawamura, T., Shimomura, O., Fukamachi, T. & Fuoss, P. H. (1981). *Acta Cryst.* A**37**, 653–658.

Lytle, F. W., Sayers, D. E. & Stern, E. A. (1989). *Physica B*, **158**, 701–722.

Maeda, H. (1987). *J. Phys. Soc. Jpn*, **56**, 2777–2787.

Nilsson, G. & Nelin, G. (1971). *Phys. Rev. B*, **3**, 364–369.

Ohtaka, O., Nagai, T., Yamanaka, T., Yagi, T. & Shimomura, O. (1998). *High-Pressure Research: Properties of Earth and Planetary Materials*, edited by M. H. Manghnani & T. Yagi, pp. 429–433. Washington, DC: American Geophysical Union.

Rehr, J. J., Mustre de Leon, J., Zabinski, S. I. & Albers, R. C. (1991). *Am. Chem. Soc.* **113**, 5135–5140.

Shimomura, O. (1996). Personal communication.

Shimomura, O. & Kawamura, T. (1987). *High-Pressure Research in Mineral Physics*, edited by M. H. Manghnani & Y. Syono, pp. 187–193. Tokyo: Terra Scientific.

Shimomura, O., Utsumi, W., Taniguch, T., Kikegawa, T. & Nagashima, T. (1992). *High-Pressure Research: Application to Earth and Planetary Science*, edited by Y. Syono & M. H. Manghnani, pp. 3–11. Tokyo: Terra Scientific.

Singh, H. P. (1968). *Acta Cryst.* A**24**, 469–471.

Stern, E. A., Bunker, B. A. & Heald, S. M. (1980). *Phys. Rev. B*, **12**, 5521–5539.

Touloukian, Y. S., Kirby, R. K., Taylor, R. E. & Lee, T. Y. R. (1970). *Thermophysical Properties of Matter*, Vol. 13, *Thermal Expansion.* New York: IFI/Plenum.

Vaidya, S. N., Akella, J. & Kennedy, G. C. (1969). *J. Phys. Chem. Solids*, **30**, 1411–1416.

Yashiro, Y., Yoshiasa, A., Kamishima, O., Tsuchiya, T., Yamanaka, T., Ishii, T. & Maeda, H. (1997). *J. Phys. IV*, **7**(C2), 1175–1176.

Yokoyama, T., Satsukawa, T. & Ohta, T. (1989). *Jpn. J. Appl. Phys.* **28**, 1905–1908.

Yoshiasa, A., Kamishima, O., Nakatsuka, A., Ishii, T. & Maeda, H. (1997). *J. Phys. IV*, **7**(C2), 1173–1174.

Yoshiasa, A., Koto, K., Maeda, H. & Ishii, T. (1997). *Jpn. J. Appl. Phys.* **36**, 781–784.

Yoshiasa, A., Nagai, T., Murai, K., Yamanaka, T., Kamishima, O. & Shimomura, O. (1998). *Jpn. J. Appl. Phys.* **37**, 728–729.